Supporting Information

UV-cured Nanocomposite Coating for Surface Charging Mitigation and Breakdown Strength Enhancement: Exploring the Combination of Surface Topographical Structure and Perfluorooctyl Chain

Chao Wang, [a] Wen-Dong Li, [a] Zhi-Hui Jiang, [a] Xiong Yang, [a] Sun Guang-Yu, [a] and Guan-Jun Zhang*

[a] State Key Laboratory of Electrical Insulation and Power Equipment, School of Electrical Engineering, Xi'an Jiaotong University, Xi'an, Shaanxi 710049, P. R. China

*Corresponding author: Email: gjzhang@xjtu.edu.cn

A. Preparation of Modified Al_2O_3 Nanoparticles

Aqueous solution of aluminum ammonium sulfate (0.1 mol / L, 500 mL), polyethylene glycol 200 (PEG 200, 8 g), emulsifier (OP-10, 3 g), and Tween 80 (3 g) were mixed and then stirred in a high speed (300 r / minutes) reactor at room temperature for 30 minutes. Then ammonium hydroxide (15 mol / L, 60 mL) was doped in the reactor. Stirring stopped when pH of the solution reached 4.5 ~ 5.0. White powders were prepared after filtrating, washing and drying (900 °C, 3 h). Chemical agents using in the experiments is listed in Table S1.

Table S1. List of chemical agents in the preparation of nanoparticles.

Name	Manufacturer	Structural formula	Molecular weight
Aluminum ammonium sulfate	Aladdin, China	$H_4S_2AlNO_8 \cdot 12H_2O$	453.33
PEG 200	Dow Chemical, USA	/	190-210
OP-10	Aladdin, China	/	/
Ammonium hydroxide	Aladdin, China	H_5NO	35.05
Tween 80	Aladdin, China	$C_{64}H_{124}O_{26}$	1309.63
Ethyl alcohol	Sinopharm Chemical, China	C_2H_6O	46.07

Surface modification of the particles were conducted by the following process: γ-Al_2O_3 flakes (30 g), isopropanol (200 g), 17-fluorodecyl trimethoxy silane (FAS 17, 18.2 g), and γ-methacryloxypropyl trimethoxy silane (KH 570, 8.6 g) were codoped in a beaker. The pH of the solution was adjusted to 5 by adding glacial acetic acid. For better uniformity, ultrasonic dispersion and high-speed stirring were adopted simultaneously during three steps: (room temperature, 2 h), (40 °C, 2 h), and (60 °C, 2 h). After cooling to room temperature, the mixture was centrifuged and cleaned by isopropanol for 3 times. Finally, the solid content was dried in a chamber to obtain modified nanoparticles with ambient temperature at 60 °C. Chemical agents using in the experiments are listed in Table S2.

Table S2. List of chemical agents in the modification of nanoparticles.

Name	Manufacturer	Structural formula	Molecular weight
KH 570	Aladdin, China	$C_{10}H_{20}O_5Si$	248.35
FAS 17	Saan Chemistry Technology, China	$C_{16}H_{19}F_{17}O_3Si$	610.39
Glacial acetic acid	Fuyu Chemical, China	$C_2H_4O_2$	60.05
Isopropanol	Aladdin, China	C_3H_8O	60.01

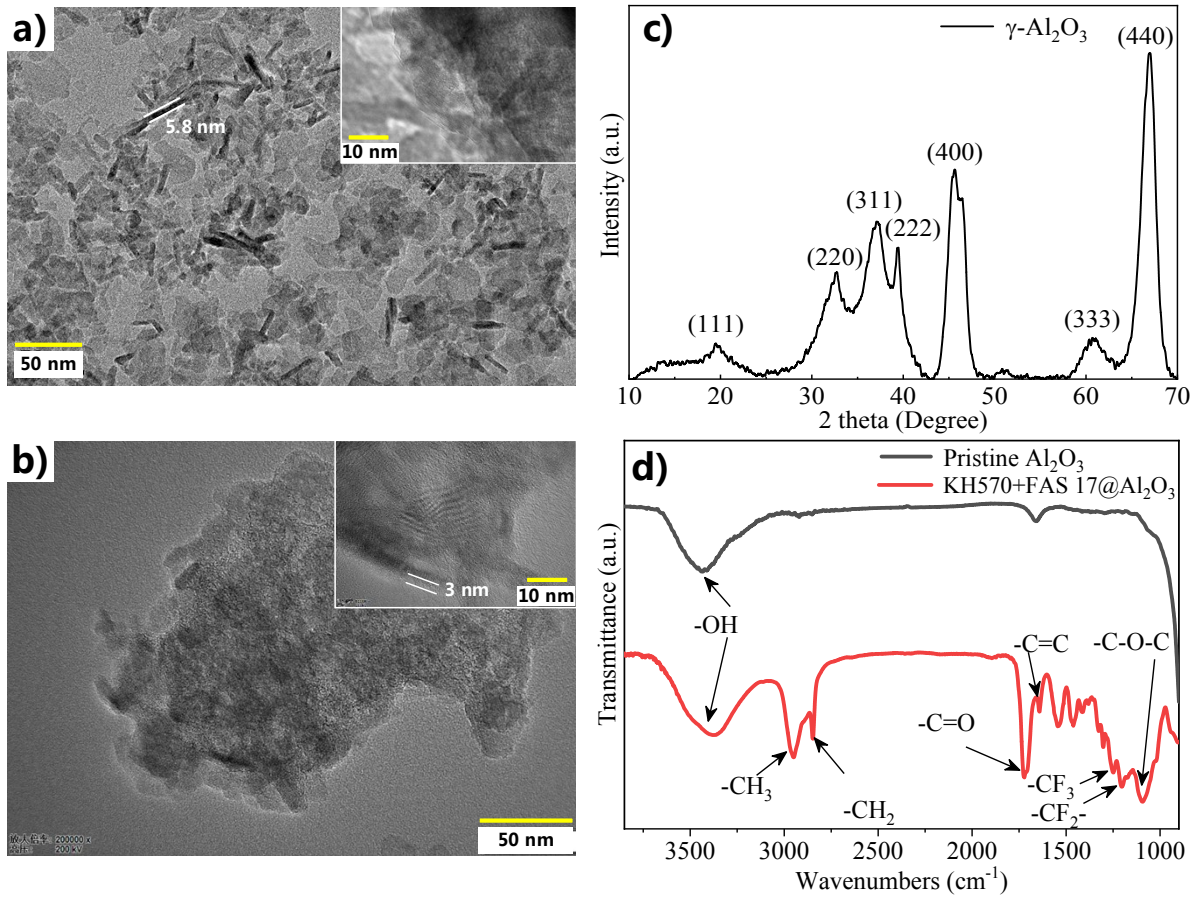

Fig. S1. TEM and XRD characterization of core-shell structured alumina nanoparticles. a) TEM characterization of nano Al_2O_3 (scale bar is 50 nm). The inset is the morphology at 10 nm scale. b) TEM characterization of KH 570 + FAS 17 @ Al_2O_3 (scale bar is 50 nm). The inset is the morphology at 10 nm scale. c), XRD and d), FT-IR curves of Al_2O_3 particles.

A statistical method using a post-processing software Image J is adopted in the measurement of the thickness of coating layer and the flake size of nanoparticles. The measurement process could be divided into three steps. Firstly, the SEM images are loaded to the Image J and the measuring scale is determined by the scalebar in the image. Then more than 50 nanoparticles are manually selected to measure the geometric parameters. Finally, the average size information is gained.

B. Preparation of Nanocomposite Coating

The coating is prepared by referencing the process shown in Fig. S2a. The modified fillers were

first dried in the vacuum chamber at 60 °C. Then UV curable resin composing of polyurethane acrylate (SD7559, Sumda New material, China), monomer (SD028, Sumda New material, China), and photoinitiator (Omnirad 184, Curease chemical, China) was codoped with modified Al_2O_3. After diluting by butyl acetate solvent, the mixture was sprayed to the surface of typical polymeric insulators like epoxy resin/Al_2O_3 composite [1], forming an uncured thin layer. Finally, the film cross-linked immediately under the radiation of UV light. Typically, UV curing process only takes a few seconds to form 3D cross-linking network. However, to guarantee high cross-linking degree, curing time in our experiments is set up as 60 s. Apart from the results shown in Fig. 2, surface morphologies of UV-F-2%, and UV-F-50% at other scales are shown in Fig. S2b and S2c, respectively. In general, the intricate geometric structure has been achieved by using nanoparticles as modifiers on both micro- and nano- scales.

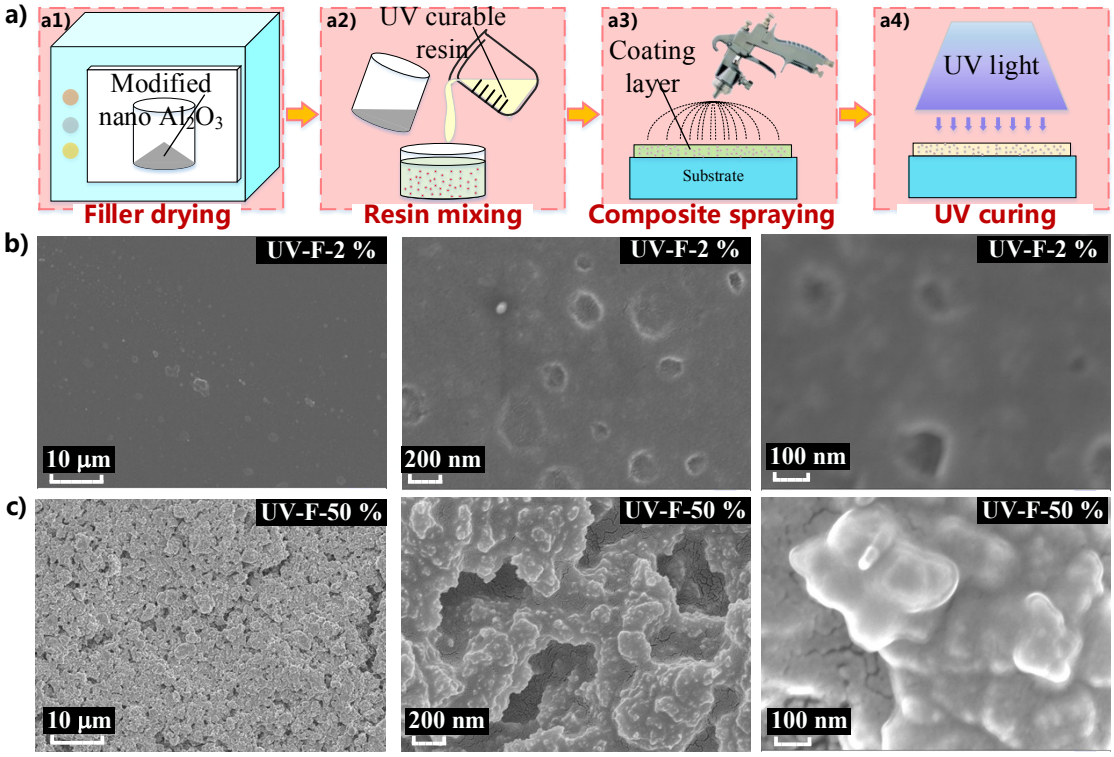

Fig. S2. Preparation and morphologies of nanocomposite coating. a) Schematic four-step preparation of nanocomposite coating. b) Surface morphologies of UV-F-2% at different scales. c) Surface morphologies of UV-F-50% at different scales.

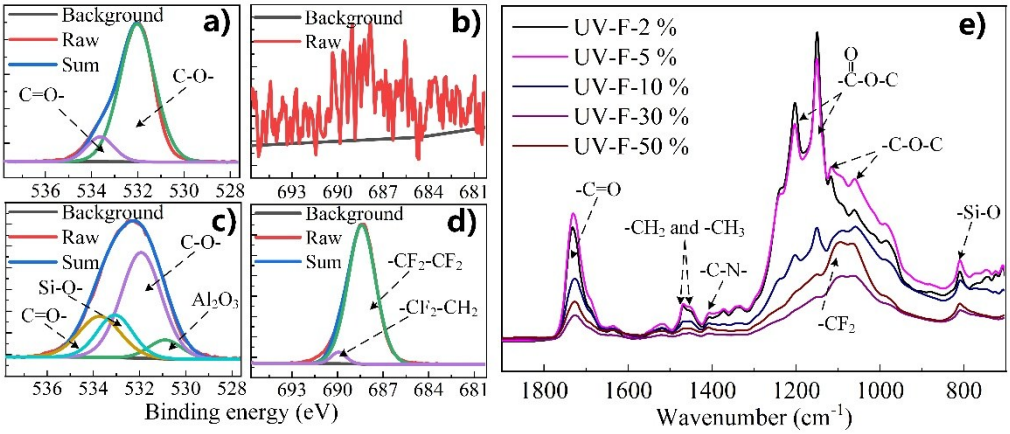

Fig. S3. Chemical characterizations of nanocomposite coating. O 1s, a) and F 1s, b) spectra of UV-F-2%. O 1s, c) and F 1s, d) spectra of UV-F-50%. b) ATF-FT-IR spectra of specimens with different loading ratios.

C. Experimental Setups for Surface Conductivity, Secondary Electron Emission, Surface Charge Behavior, and Electrical Strength Characterization

As shown in Fig. S4, after applying a fixed voltage (400 V) to the specimen, the stable current flowing through the surface was recorded by 6517B after 6 minutes at 298 K. Surface conductivity (ρ_s, Ω) of the coating was then calculated in the software through the following equation:

$$\rho_s = 53.4 \cdot \frac{U}{I} \tag{1}$$

where U represents the applied voltage, and I indicates the current recorded by ampere meter.

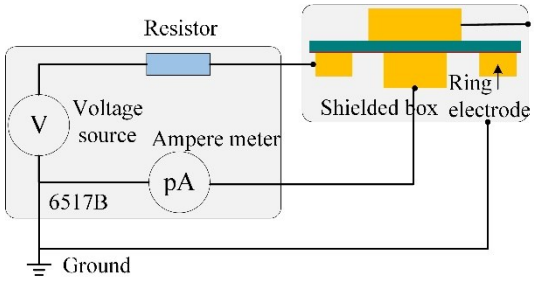

Fig. S4. Diagram of surface conductivity measurement.

The measurement system of secondary electron yield (SEY) is demonstrated in Fig. S5. In general, the system can be mainly divided into two parts: one is the sample delivery chamber

and the other is the measuring chamber. The measurements of SEY were performed in the measuring chamber with an electron gun producing an electron beam with energies from 50 eV to 5 keV and beam current up to 100 nA. In the experiments, the beam current was set as 20 ~ 50 nA and the pressure in the chamber was lower than 5×10^{-4} Pa. The electron gun was operated in the pulsed mode and the pulse duration was set as 1 ms. The primary electrons were collected by a double-deck metal net, and the primary current was amplified by a current amplifier and then measured by the oscilloscope. The secondary electrons were collected by a Faraday cup made with an inside of graphite. Similarly, the secondary current was amplified by a current amplifier and then measured by the oscilloscope. The SEY (δ) is the ratio of secondary current (I_s) and primary current (I_p) [2]. That is

$$\delta = \frac{I_s}{I_p} \tag{2}$$

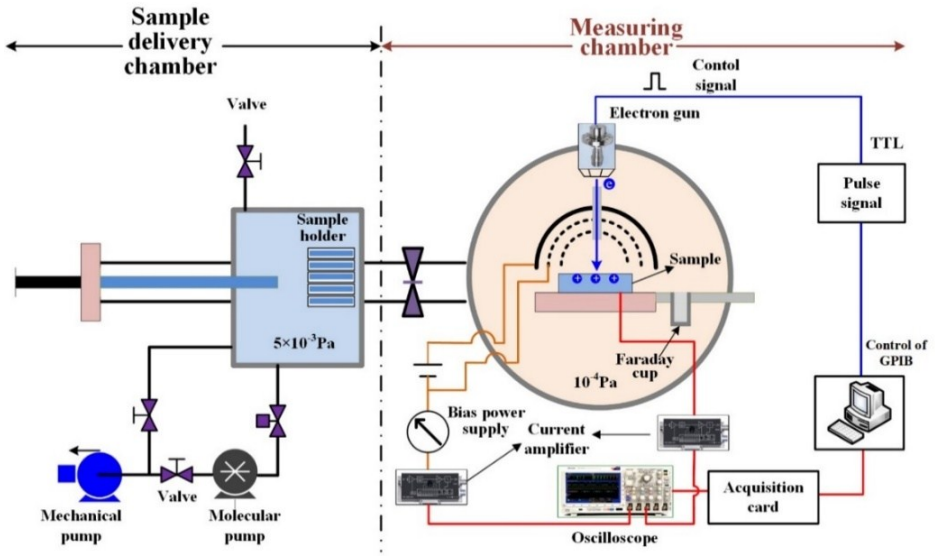

Fig. S5. Measurement system of secondary emission yield [2].

Pulsed flashover in vacuum or atmosphere was implemented at a self-designed platform. A schematic of the surface breakdown measurement and the corresponding characterization strategy are shown in Fig. S6. The negative impulse voltage waveform generated by the circuit in Fig. S6a is demonstrated in the blue dashed box in Fig. S6c. The peak value of the impulses is up to -80 kV, and the front time (T_f), 1/2 peak time (T_t) of the waveform are 1.2 and 43 μs,

respectively. The sizes of the electrode and prepared specimens used for the study are shown in Fig. S6b. Three voltage indexes (i.e., the first breakdown voltage (U_{fb}), conditioned voltage (U_{co}), and hold-off voltage (U_{ho})) were conventionally used to evaluate the surface flashover characteristics of the testing specimens at different stages. As shown in Fig. S6c, at each voltage level, the impulse voltage was applied five times to the specimen; U_{fb} represents the voltage at which the flashover first occurs, while U_{co} and U_{ho}, respectively represent the voltages at which the flashover occurs and then disappears during each of the five times.

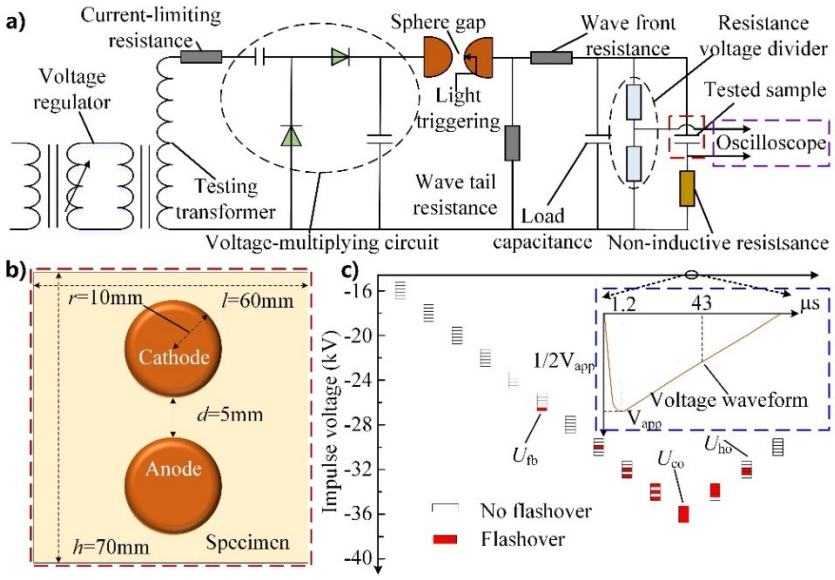

Fig. S6. Experimental setup for flashover strength characterization. a) Schematic of vacuum flashover circuit. b) Electrode structure. c) Characterization strategy [3].

Based on the surface flashover measurement platform, a Kelvin probe along with electrostatic voltmeter were utilized for surface potential distribution measurement. The layout of this experiment is shown in Fig. S7. After applying impulse voltage to the specimen, displacement platform moved along the preset route at the specimen's surface, scanning a region with an area of 48×30 mm. The data was recorded by electrostatic voltmeter and then uploaded to the computer by an A/D converter. Notably, after positioning to the supporter, the specimen was cleaned by ethanol and then dried in air dry oven to avoid influence of residual charge caused by triboelectrification.

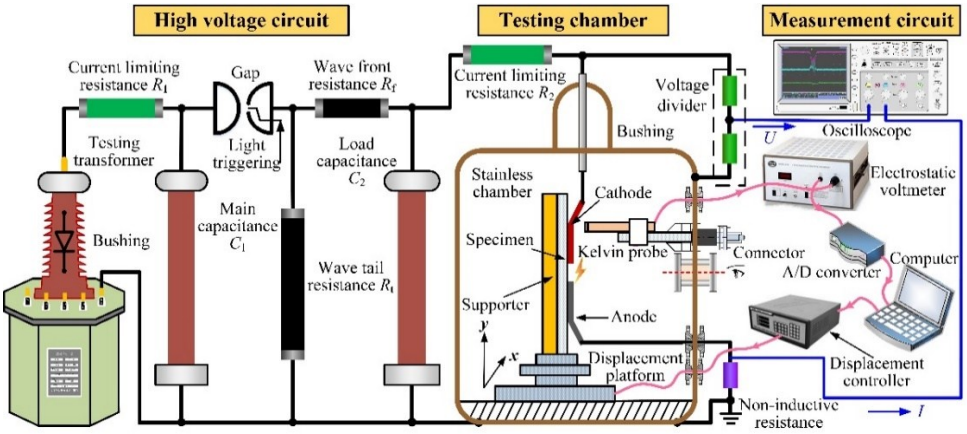

Fig. S7. Experimental setups for surface potential measurement [4].

Documents containing surface potential information were reconstructed by MATLAB software. Specially, to remove the noise caused by probe vibration, a de-noised process using second order nonlinear interpolation filter was performed before plotting surface potential distribution.

Experimental setup for surface charge decay characterization is shown in Fig. S8. DC high voltage (HV1, 15 kV) was applied to the needle electrode. Strong *E* field near the needle electrode caused consecutive gas ionization; then, the electrons migrated to the dielectric surface under the force of the electrical field between the mesh and the ground electrode. The negative charges deposited on the insulator's surface decreased the surface potential leading to a decrease in the potential difference between the mesh and dielectric surface, which terminated the migration process.

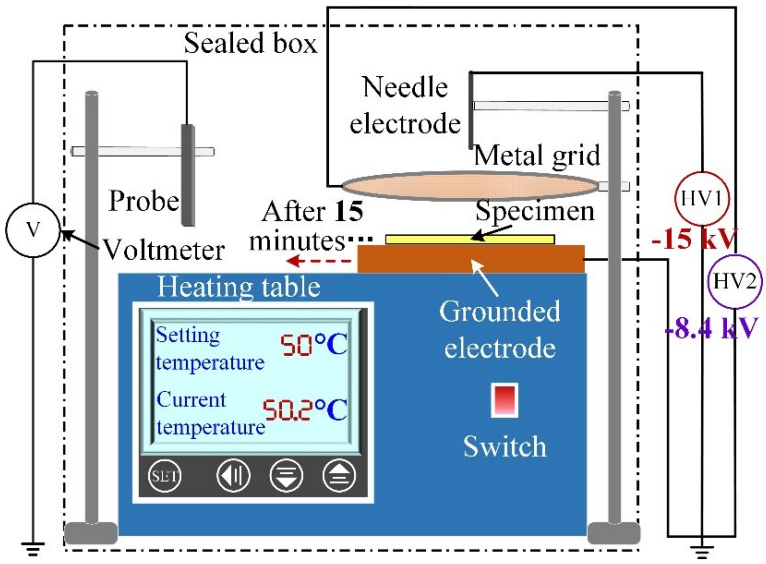

Fig. S8. Experimental setup for surface charge decay rate measurement in air

Table S3 describes the changes of surface roughness and electrical resistivity with filler's loading ratio. In general, with the increase of loading ratio, surface roughness gradually increases while surface electrical resistivity shows a declining trend.

Table S3. Surface roughness and electrical resistivity.

Type	Surface roughness (R_a, μm)	Surface electrical resistivity (Ω)
UV-F-2%	0.067	6.18×10^{16}
UV-F-5%	0.090	2.64×10^{16}
UV-F-10%	0.591	7.21×10^{15}
UV-F-30%	0.966	8.94×10^{12}
UV-F-50%	1.130	4.68×10^{12}

Figure S9 supplements the surface potential distribution of UV-F-50% at -45 kV. It's notable that surface potential improved with the increase of impulse times. But invariably, the maximum values of surface potential are all below 4 kV, indicating that the amount of surface charge still maintains at a very low level.

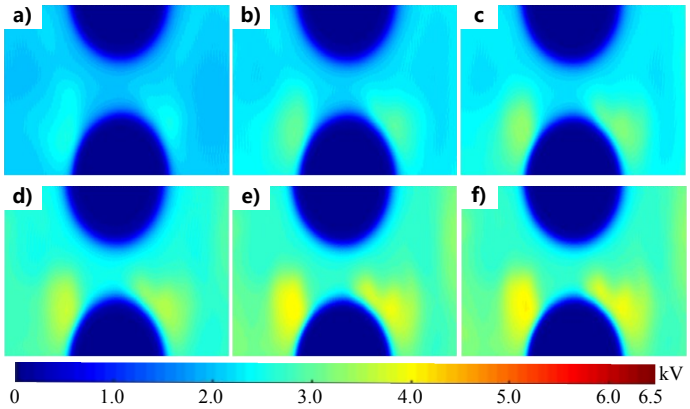

Fig. S9. Surface charge accumulation of UV-F-50% at -45 kV. a) ~ f) respectively, *N*=1, 5, 10, 50, 100, 200.

References:

[1] J.Y. Xue, J.H. Chen, J.H. Dong, H. Wang, W.D. Li, J.B. Deng, G.J. Zhang, *J. Phys. D-Appl. Phys.*, 2019, **52**, 14.

[2] R.D. Zhou, G.Y. Sun, B.P. Song, B.H. Guo, N. Yang, H.B. Mu, G.J. Zhang, *J. Phys. D-Appl. Phys.*, 2019, **52**, 375304.

[3] C. Wang, W.D. Li, J. Guo, X. Chen, Z.-H. Jiang, X.R. Li, B.H. Guo, G.J. Zhang, *Appl. Surf. Sci.*, 2019, **144432**.

[4] B.H. Guo, G.Y. Sun, S. Zhang, J.Y. Xue, R.D. Zhou, B.P. Song, H.B. Mu, G.J. Zhang, *J. Phys. D-Appl. Phys.*, 2019, **52**, 215301.